Hydrogen donation of bio-acids over transition metal facets: A Density Functional Theory study

Jiajun Zhang[ac], Xiaolei Zhang[ac,]*, Amin Osatiashtiani[b], Anthony Bridgwater[b]

* Corresponding author: X.Z., E-mail address: xiaolei.zhang@strath.ac.uk

[a] Department of Chemical and Process Engineering, University of Strathclyde, Glasgow, United Kingdom

[b] European Bioenergy Research Institute (EBRI), School of Engineering and Applied Science, Aston University, Aston Triangle, Birmingham, B4 7ET, United Kingdom

[c] School of Mechanical and Aerospace Engineering, Queen's University Belfast, Belfast, United Kingdom

Abstract

This research aims to evaluate and systematic compare two bio-based acidic hydrogen donors as alternative hydrogen source for hydrodeoxygenation (HDO) of bio-oil from fast pyrolysis of biomass. We investigated the hydrogen donation performance of acetic acid (AcOH) and formic acid (FA) over the most stable facet of transition metal in comparison with the dissociation of H_2, using Density Functional Theory (DFT) modelling. It was found that AcOH adsorbed more strongly on Mo (110) than the other base transition metals investigated. The binding of both acid molecules and Mo were dominated by electrons migration from the molecule to the metal, while electron enrichment was also observed for FA during the adsorption. The bonds strength for both acids were weakened by Mo, therefore, facilitating their decomposition. The hydroxyl hydrogen and one methyl hydrogen of AcOH could be readily cleaved with low energy barriers, but the methylene hydrogen was found to be difficult to cleave when the carbon was unsaturated. Within the FA molecule, the hydroxyl hydrogen would be donated more readily than the hydrogen from aldehyde group. H_2 dissociated during adsorption on the Mo (110) facet with negligible energy barrier. Within the three sources of hydrogen (acetic acid, formic acid and H_2 gas), H_2 gas has the advantage of easy dissociation when compared to the hydrogen generated from biomass-derived acids (bio-acids). However, the large enthalpy change resulted from the exothermic decomposition of the bio-acid will probably facilitate the activation and further migration of the single H atom for donation over the metal facet compared to H_2 gas. AcOH exhibited a greater potential than FA as a hydrogen donor over Mo (110) due to the release of more H atoms with low energy barriers. The modelling results also suggested that AcOH is a promising alternative hydrogen source to replace H_2 gas over the facet of Mo (110).

Abbreviations: Acetic Acid, AcOH; Formic Acid, FA; Aromatic Hydrocarbons, AHs; Electronic density difference, EDD

Key words: Hydrogen donor compounds; Catalytic decomposition; Hydrodeoxygenation; DFT modelling; Transition metals

1. Introduction

Nowadays biofuel is an attractive alternative fuel because it can lower our dependency on conventional fossil fuels, achieve “zero” net carbon emissions, and tackle the challenge of global warming [1]. Thermochemical conversion of waste biomass via catalytic fast pyrolysis offers a promising route to biofuels. However, the direct use of bio-oil is hindered by its undesirable physicochemical properties such as low calorific value due to its high oxygen content and water content, high viscosity and low stability owing to its high acid content. This explains why upgrading is being so intensively studied.

Hydrodeoxygenation (HDO) is considered an effective method for upgrading bio-oil to more valuable and useful liquid products [2]. Conventionally, molecular H_2 gas is used in industrial HDO processes, because of its dissociation on the surface of the catalysts, thus providing high reactivity. However, there are some drawbacks associated with the application of molecular H_2 gas such as the high process costs due to high-pressure reactors, concerns over process safety regarding H_2 storage and utilisation, the requirement to recover and recycle hydrogen. Additionally, using pure H_2 during HDO may lead to the saturation of aromatic rings, producing undesired cycloalkanes instead of aromatic hydrocarbons. Therefore, alternative sustainable hydrogen sources are urgently sought-after to address the challenges of developing an efficient and cost effective HDO process.

Much effort has been devoted to finding the alternative hydrogen sources, and it has been reported that hydrogen can be produced in-situ via various reactions [2,3]. Commonly reported alternative hydrogen donors include primary and secondary alcohols such as methanol, ethanol and isopropyl alcohol (IPA), carboxylic acids including acetic acid (AcOH) and formic acid (FA), and aromatic hydrocarbons (AHs) including tetralin and decalin [4,5]. These hydrogen-rich compounds can supply hydrogen for the HDO reaction through self-decomposition or dehydrogenation [1]. For example, Wang et al. [6,7] reported the deoxygenation of phenol over Ni/Al_2O_3 and Ru based catalysts using methanol and formic acid as hydrogen donor compounds. Guo et al. [8] explored the HDO of p-cresol over a Ru based catalyst with IPA as the hydrogen donor, achieving 98.5% conversion and 84.0% yield of toluene. IPA was also found to be effective in humins conversion [9]. Vasiliadou and Lemonidou reported the HDO of glycerol at 220 – 250 °C. The highest 1,2-propanediol yield of 53% was obtained using ethanol as the source of hydrogen [10]. Pajak et al. [11] investigated the hydrogen transfer from tetralin and decalin to coal derived tars, revealing hydrogen transfer from decalin was two times greater than that of tetralin. Similar conclusions were drawn by other researchers when decalin and tetralin were used for bio-oil upgrading through hydrogen transfer deoxygenation [12,13]. In-situ H_2 gas production can also take place through redox reactions. For example, water-gas shift reaction ($CO + H_2O \rightleftharpoons CO_2 + H_2$) may occur within the HDO process to supply hydrogen [14].

The mechanism of various hydrogen transfer reactions for HDO have been extensively investigated [15–18]. The adsorption and dissociation of molecule hydrogen over various transition metals were reported by Pozzo et al., indicating Ni was the most effective metal in such a process [19]. Experimental and modelling investigation performed by Grilc and Likozar and other researchers revealed that bi-functional Ni-Mo based catalysts are promising for HDO with molecular H_2 [20,21]. Numerical models have been reported as well [22–24] to describe the mechanism and kinetics of catalytic HDO reactions.

DFT based studies regarding decomposition of bio-alcohols have been also intensively reported; the decomposition mechanism of methanol over Co(0001) and Co(111), Pd(111), Pt(111), and Ni(111) facets has been investigated, predicting all the C-H bond and C-O bond would cleave prior to the CO bond in these scenarios [25,26]. Alcalá et al. reported the decomposition mechanism of ethanol, predicting that demethylation reaction would happen much faster than dehydroxylation over Pt(111), and methane and CO were more likely to be produced [27,28]. In addition, detailed mechanisms for ethanol decomposition over various transition metals, propanol decomposition over Ni-Fe and Ni-Cu bimetallic facet, and butanol decomposition over Pd(111) facet have been widely reported [28–31].

There are limited reports on the DFT modelled decomposition of AHs (as H donors). Kim et al. elucidated the dehydrogenation mechanism of decalin to tetralin and further to naphthalene on the (111) facet of Pd and Pt respectively, revealing that according to the modelling, Pd would outperform Pt by lowering the energy barrier of tetralin conversion to naphthalene by 0.31 eV [32].

Regarding the bio-acids, the decomposition of FA over Cu (111) facet has been analysed by DFT, predicting the most favourable reaction pathway was HCOOH → HCO → CO [33]. The decomposition of acetic acid over a variety of catalysts were also reported [34,35]. Xinbao et al. investigated the decomposition mechanism of AcOH over Co (111) stepped facet, and revealed that the reaction pathway follows $CH_3COOH \rightarrow CH_3CO \rightarrow CH_2CO \rightarrow CH_2 \rightarrow CH$ [36]. Although, there are other different reaction mechanisms for AcOH decomposition proposed in the literature [37–39]. The detailed description of the decomposition of bio-acids over different catalysts, especially over base transition metals, are still unclear and scarce. Moreover, previous studies have reported the performance of various hydrogen donors, however most of them cannot be compared because different catalysts were used. There are very few reports on the evaluation of the reactivity of different hydrogen donor compounds over one selected catalyst and their capacity for HDO reactions.

Hence, this research is aimed at the evaluation and systematic comparison between two bio-based acidic hydrogen donors, since they abundantly exist in the primary bio-oil. The decomposition of these carboxylic acids leads to in-situ hydrogen formation, which subsequently can take part in HDO reactions. With respect to catalyst selection, the performance of noble metal based catalysts e.g. Pt and Ru, have been widely studied, while not enough attention have been paid to the base transition metals. Therefore, this study has sought to predict the decomposition of AcOH with a focus on the cleavage of hydrogen related bonds over various transition metals. Ten transition metals (Ni, Mo, Fe, Co, Pt, Rh, Ru, Zn, Cu, and Pd) are compared regarding their binding energy in adsorbing AcOH and the one with strong binding was selected. Then, AcOH and FA are compared with H_2 in terms of their adsorption process and hydrogen donation performance over the most stable facet of the selected catalyst. Electronic density difference (EDD) of the hydrogen donor compounds was analysed to investigate the interface interactions. Bond lengths of the donor compounds were also tracked throughout their decomposition to evaluate the impact of metal catalyst.

2. Computational details

The first-principle density functional theory plus dispersion (DFT-D) calculations were implemented in the Cambridge Sequential Total Energy Package (CASTEP) module available in Materials Studio 2017 R2 from BIOVIA [40,41]. The generalized gradient corrected approximation (GGA) [42] treated by the Perdew−Burke−Ernzerhof (PBE) exchange-correlation potential with long-range dispersion correction via Grimme's scheme was used to calculate the exchange-correlation energy [43]. The On-the-fly generated (OTFG) ultrasoft pseudopotential was employed as the scheme in the representation of reciprocal space for all the elements [44,45]. The plane-wave cut-off energy was set to 500 eV for all the calculations based on its independence test (Fig. S1(a)). The Brillouin zone was sampled using a 2×2×1 Monkhorst-Pack k-point (spacing of 0.04 $Å^{-1}$) with a smearing of 0.1 eV, based on its independence test (Fig. S1(b)). The self-consistent field (SCF) tolerance was set to 10^{-6} eV/atom. All the modelling was performed with a convergence threshold of 10^{-5} eV/atom on energy, 0.03 eV/Å on maximum force, and 10^{-3} Å on the maximum displacement. No symmetry constraints were used for any modelling. The impact of zero point energy (ZPE) was evaluated for the adsorption of AcOH and FA. It was found that the net ZPE corrections (difference between ZPE of the systems before and after the adsorption) were less than 0.01eV, so that the ZPE correction was not included in the calculations of this study. The computational method is believed to give high precision results, according to the validation of lattice constant for each metal element lattice in this study; the variations between computational and experimental values are less than 0.10 Å for most systems (full comparison is shown in Table S1).

The most stable facets of the ten metals were simulated; facet (1 1 1) was simulated for face-centred cubic (FCC) metals including Ni, Cu, Pd, Pt, and Rh, and facet (1 1 0) was simulated for body-centred cubic (BCC) metals of Mo, Fe. For hexagonal close-packed (HCP) metals including Co, Zn, and Ru, facet (0 0 1) was simulated [28,46]. All the metal facet models were created from the optimized metal lattices, and a four-layer slab of P (5×5) super-cell was used with the adsorbate coverage of 1/25ML (Fig. S2). 15Å vacuum region was created above the metal facet. The transition state (TS) was completely determined by the LST/QST method, and the TSs for the dominated reaction steps were confirmed by the unique imaginary frequency. Mulliken charges were assigned to each bond to address the bond order [47]. The adsorption energy E_{ad} was determined by Eq.1, where $E_{catalyst}$, $E_{adsorbate}$ and $E_{adsorbate/catalyst}$ are the total energies of clean metal facet, free adsorbate molecule and metal facet with adsorbed molecule respectively. The energy barriers of reactions $E_{barrier}$ were determined by the difference between the transition state and reactant energies, as shown in Eq.2, where $E_{transition\ state}$ and $E_{reactant}$ are the total energies of the transition state and reactant of a reaction.

$$E_{ad} = E_{catalyst} + E_{adsorbate} - E_{adsorbate/catalyst} \tag{Eq.1}$$

$$E_{barrier} = E_{transition\ state} - E_{reactant} \tag{Eq.2}$$

EDD was determined by Eq.3.

$$\Delta\rho = \rho_{adsorbate@Mo(110)} - (\rho_{adsorbate} + \rho_{Mo(110)}) \tag{Eq.3}$$

where $\rho_{adsorbate@Mo(110)}$ is the electron density of the total adsorbate + Mo(110) system, and $\rho_{adsorbate}$ and $\rho_{Mo(110)}$ are the unperturbed electron densities of the adsorbate and the Mo(110) facet, respectively.

Geometry optimization was implemented to every model before energy was calculated. Energy of all the geometries was calculated at 0K in the DFT investigation.

3. Results and discussion

3.1 Metal catalyst selection based on AcOH adsorption

Most stable facets of ten transition metals were established to identify the metal catalyst that can adsorb AcOH more strongly than the others. The adsorption modelling was carried out by placing AcOH molecule vertically, and binding onto the top site of each metal facet with the carbonyl oxygen atom. More details of the stable adsorption models are shown in the Fig. S2. The adsorption energies are summarized in Table 1, along with relevant geometry parameters (bond length of O-metal, which refers to the distance between the centres of the bounded oxygen atom and the nearest metallic atom, and the corresponding angle of C-O-metal) of the most stable geometry.

Table 1. Adsorption energies and geometrical parameters of AcOH on common facets of transition metals

Metal facets	Bond length (Å)	∠C-O-metal (degree)	Adsorption energy (eV)
Ru (0001)	2.16	143.22	0.91
Mo (110)	2.10	170.16	0.88
Ni (111)	1.93	169.33	0.71
Pd (111)	2.14	141.28	0.70
Fe (110)	1.97	170.92	0.67
Co (0001)	1.95	176.82	0.66

Rh (111)	2.21	175.10	0.60
Pt (111)	2.32	137.75	0.58
Cu (111)	2.15	148.03	0.47
Zn (0001)	2.72	127.95	0.30

Note: Considering the effects of adsorption sites and compounds configurations on adsorption energy, more comprehensive adsorption energy of AcOH onto the top three metal facets of Ru, Mo and Ni in different adsorption sites and configurations are calculated and shown in Table 2 and Table. S2.

The adsorption energy of AcOH onto all of the modelled transition metals facets were less than 1.00 eV. The highest adsorption energy of 0.91 eV and 0.88 eV associated with AcOH adsorption onto Ru (0001) and Mo (110) respectively, followed by 0.71 eV for Ni (111) and 0.70 eV for Pd (111). Adsorption of AcOH on Zn (0001) exhibited the lowest adsorption energy of 0.3 eV. The bonds generated between metal facets and AcOH molecule ranged from 1.93 to 2.72 Å, and the angles generated between C-O bond and O-metal bond ranged between 127.95° and 176.10° for all cases.

In the perspective of thermodynamic, the high adsorption energy for Ru, Mo, Ni, Pd implies that chemisorption happens with a strong binding between AcOH molecule and the metals facets. These four metals are commonly known as the catalysts being adopted for the HDO using H_2 gas and for the decomposition of organic compounds with good performance [5,48–50]. Specifically for acids decomposition, Ru, Ni and Pd have been widely reported based on experimental investigation as well as DFT modelling [6,7,34,39,51]. Ru was found quite active in HDO with formic acid as hydrogen donor [7]. Ni was reported to exert high activity in HDO with H_2 gas but poor performance with formic acid as hydrogen donor [6]. Pd is also active but has the potential to lead to the direct formation of CH_4 instead of hydrogen donation [34]. Besides, Ru and Pd are noble metals, which would lead to high cost. In comparison, Mo as catalyst has been less investigated thus it is the focus for the further investigations in this study.

3.2 AcOH as hydrogen donor on Mo (110) facet

The adsorption of AcOH onto Mo (110) facet is investigated in terms of the preferred absorption sites and configuration. Four probable adsorption sites are considered for the adsorption modelling, including top site (Top), short bridge site (SB), long bridge site (LB) and hollow site, as shown in Fig. 1.

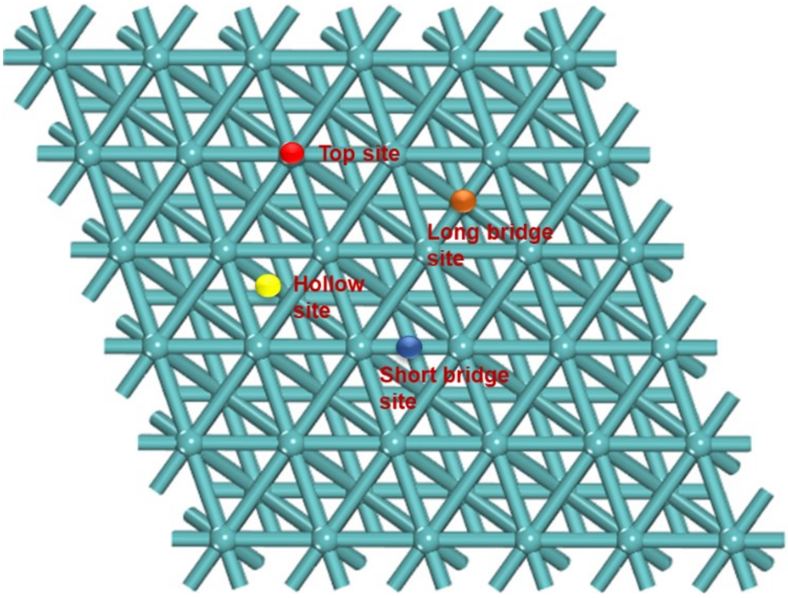

Fig. 1. The probable adsorption sites on the facet of Mo (110)

The adsorption of AcOH was simulated over four different adsorption sites, and four configurations for AcOH were compared. The structures of each stable adsorption are shown in Table 2.

Table 2. Adsorption energy of AcOH, FA and H_2 onto Mo (110) at different sites and configurations

Adsorption Energy of AcOH (eV)	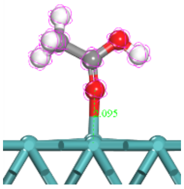 ① O_α-Mo	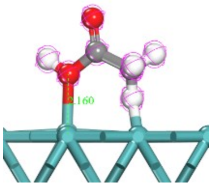 ② O_β-Mo	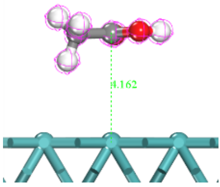 ③ Parallel	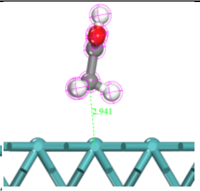 ④ C_α-Mo
Top	0.88	0.70	0.28*	0.22*
Short Bridge (SB)	1.24	-	-	-
Long Bridge (LB)	0.28*	-	-	-
Hollow	0.95	-	-	-

Adsorption Energy of FA (eV)	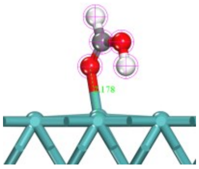 ① O_α-Mo	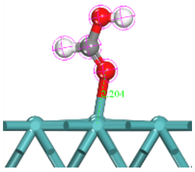 ② C-Mo**	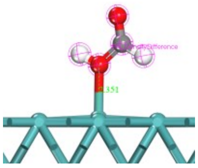 ③ O_β-Mo	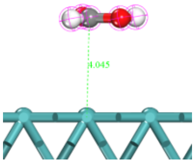 ④ Parallel
Top	1.15	0.75	0.51	0.18*
Short Bridge (SB)	0.15*	-	-	-
Long Bridge (LB)	0.16*	-	-	-
Hollow	0.12*	-	-	-

Adsorption Energy of H_2 (eV)	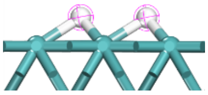 ① Parallel	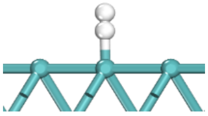 ② Vertical		
Top	0.57	0.56	-	-
Hollow	1.64	-	-	-

* Only stable physical adsorption observed

** Transformed binding from C-Mo to O-Mo (as shown) after geometry optimization

Configuration ① led to the highest AcOH adsorption energy of 0.88 eV compared to other configurations, followed by configuration ④, for 0.70 eV. While configuration ② and ③ resulted in lower adsorption energies of 0.28 eV and 0.22 eV respectively. Regarding different adsorption sites based on configuration ①, AcOH was able to develop strong bindings on to the top, SB and hollow site of Mo facet, resulting in the adsorption energy of 0.88 eV, 1.24 eV and 0.95 eV respectively. The adsorption of AcOH onto LB site gave rise to the adsorption energy of 0.28 eV.

The results reveal that AcOH molecule most likely will adsorb on the SB site of Mo (110) facet through the binding between O^{α} and Mo facet, leading to the highest adsorption energy. Carbon and hydrogen in the molecule are found hardly to form strong bond with the Mo facet independently. The adsorption onto the positions of Top ① and SB ②, and hollow are likely to be chemical adsorption, because of the large adsorption energy. To confirm this, electrons migration between the interfaces was investigated by the calculation of EDD, as shown in Fig. 2.

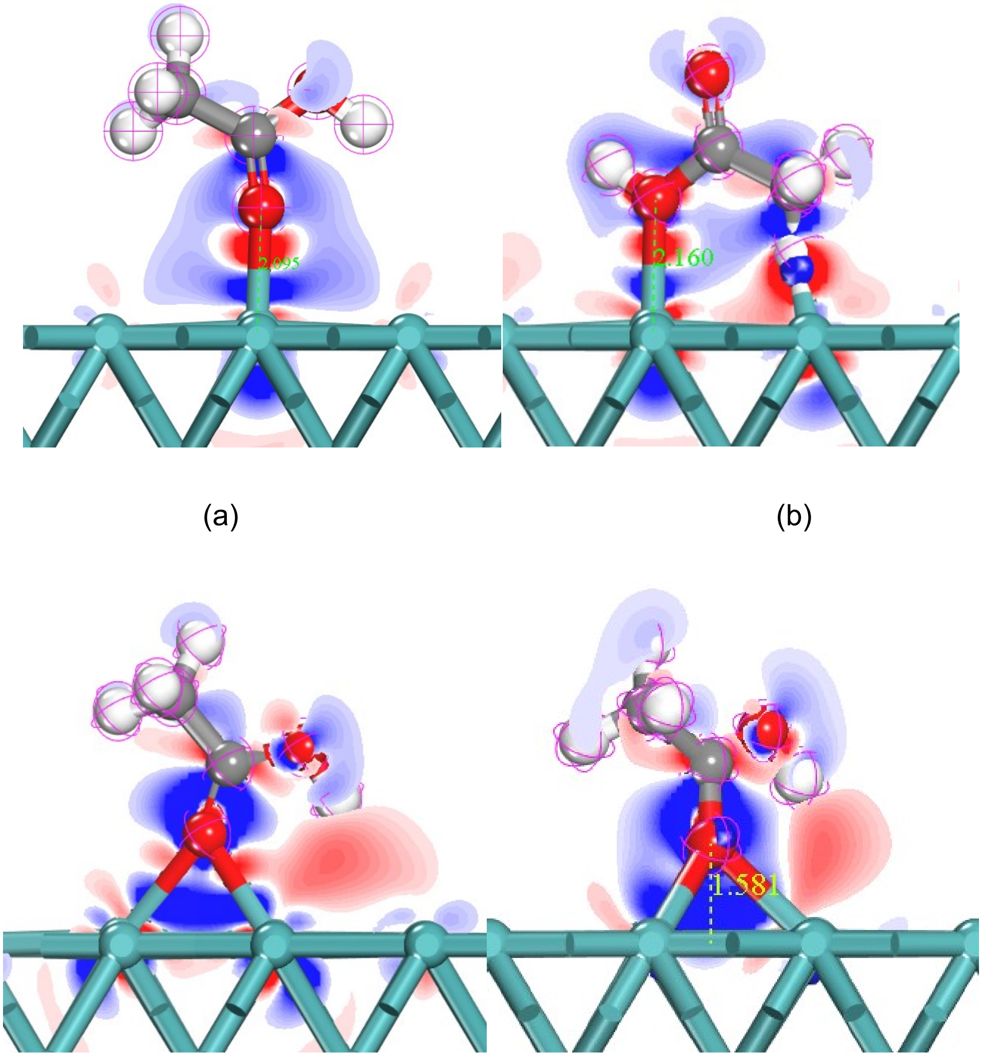

(a) (b)

(c) (d)

Fig. 2. Colour mapping of electron density difference (threshold value: +/- 0.05 electrons/Å^3) for AcOH adsorption configurations of (a) Top ①, (b) Top ②, (c) SB, and (d) hollow. (Loss of electrons is indicated in blue, while electron enrichment is indicated in red)

Obvious electrons migration around the interfaces of the above four adsorptions indicates that chemical adsorption happened. The adsorption was likely to happen via O^{α}, where was also the centre for electron migration. When only O^{α} atom (Fig. 2(a) and (b)) bonded to the facet, fewer electrons were lost but apparent electrons enrichment was observed around the O^{α} atom (Fig. 2(a)) and around the adsorbed hydrogen atom (Fig. 2(b)). However, severer electron loses happened when AcOH bound to two Mo atoms through O^{α} atom over the SB and hollow positions (in Fig. 2(c) and (d)). These results are in agreement with the highest adsorption energy on these two sites. They also reveal that the stable adsorption of AcOH on Mo (110) is achieved by strong electron migration from the molecule to the substrate through the bridge of C^{β}- O^{α}-Mo.

During modelling the decomposition of AcOH over Mo (110), the cleavage energy and reaction enthalpy were also calculated, in comparison with the free molecular decomposition of AcOH molecule in the absence of metal catalyst, which is shown in Fig. 3. The most favourable decomposition pathway of AcOH is illustrated in Fig. 4. The bond lengths and bond orders for the AcOH molecule and its most probable intermediates during the decomposition are shown in Table. S3 (a) and (b).

For the free molecular decomposition of AcOH, the C^{β}-O^{α} bond showed the largest cleavage energy of 8.46 eV, which was followed by the C^{α}-H bond with 5.85 eV and the C-C bond with 5.17eV. The bonds of O^{β}-H bond and C^{β}-O^{β} exhibited similar cleavage energy of 4.51 eV and 4.67 eV respectively. All the cleavage reactions in free molecular decomposition were endothermic as there was no new bond formed.

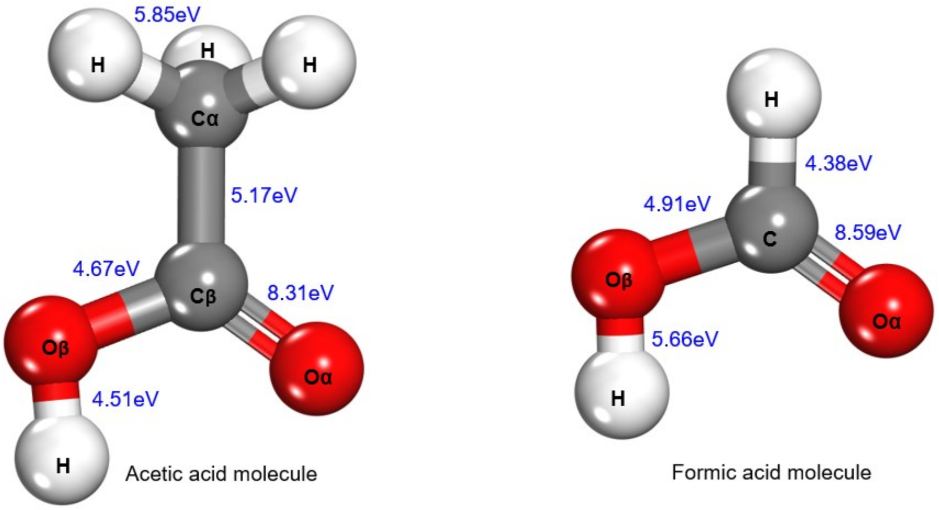

Fig. 3. The cleavage energy for the free molecular decomposition of AcOH and FA

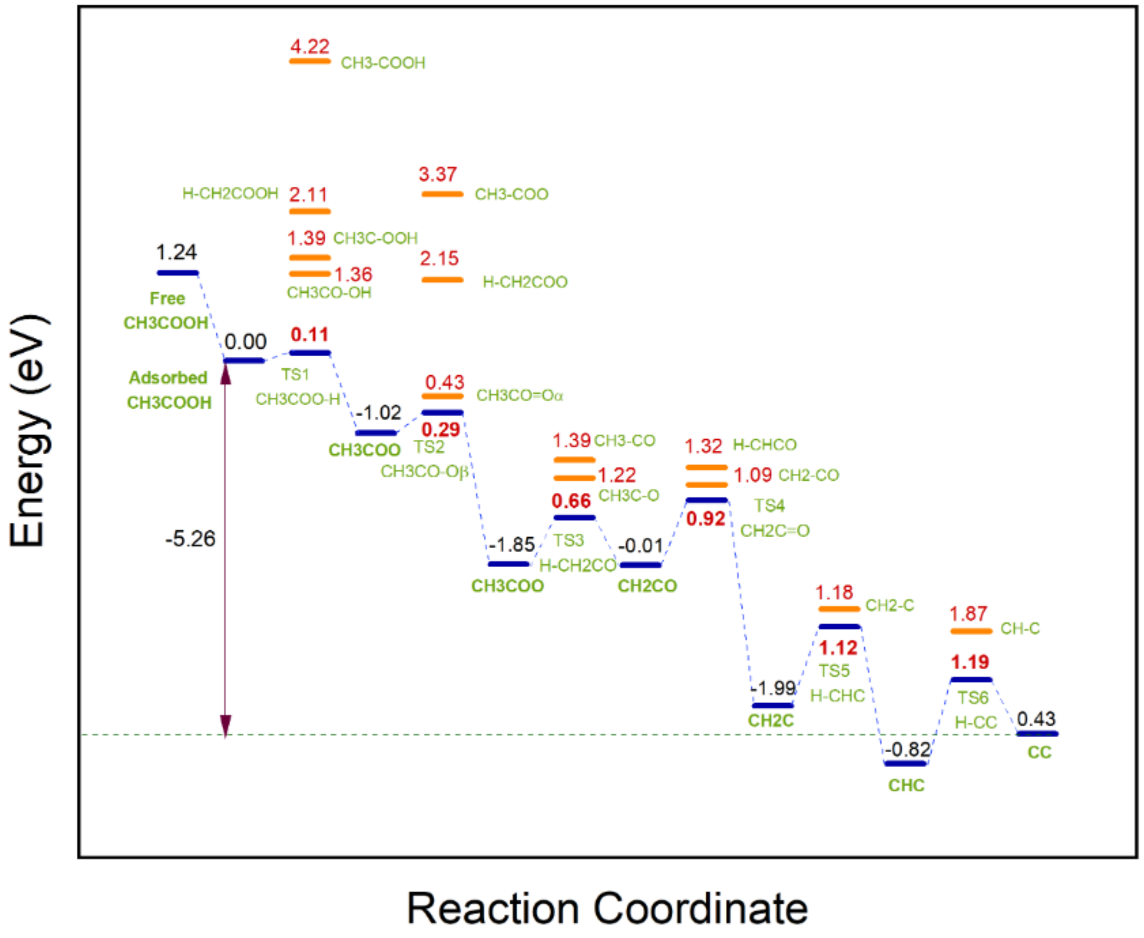

Fig. 4. The decomposition pathways of AcOH over Mo (110) facet

The decomposition of AcOH over Mo facet was the most likely to start with the cleavage of the hydroxyl group with a small energy barrier of 0.11 eV, producing acetate and one H atom. The acetate could then lose the O^{β} atom and one H sequentially to form CH_2CO. All the cleavage reactions in the decomposition of AcOH over Mo facet were exothermic, except for the final H-CC cleavage step, which was endothermic with $\Delta H = 0.43$ eV.

The reaction modelling results reveal that the bulk decomposition of AcOH over Mo (110) is exothermic, which is much more thermodynamically favoured compared to its free molecular decomposition. Besides, the significant decrease in cleavage energy observed during the catalytic decomposition indicates the excellent effect of Mo facet in facilitating the cleavage of AcOH. The most favourable decomposition pathway of AcOH over Mo (110) is $CH_3COOH \rightarrow CH_3COO+H \rightarrow CH_3CO+O+H \rightarrow CH_2CO+H+O+H \rightarrow CH_2C+O+H+O+H \rightarrow CHC+H+O+H+O+H \rightarrow CC+2H+O+H+O+H$, which is similar to the reported decomposition pathways [36]. The highest energy barrier of 1.19 eV among all the elementary reactions implies that the decomposition of CHC to CC is the rate-determining step. It is also found that the decarboxylation of CH_3COO was suppressed at the beginning, and hydrogen is released during the whole decomposition process. The C-C bond is stable throughout the decomposition, and the remaining C-C anchoring on the Mo facet would result in carbonaceous deposits after further accumulation or they crack to produce CO_2 & CH_4 with hydrogen and oxygen generated in previous steps [34].

3.3 FA as hydrogen donor on Mo (110) facet

The adsorption energies of FA onto the four different adsorption sites and in four different configurations are specified in Table 2. The configurations with the binding of O^{α}-Mo (① and ②) showed the highest adsorption energy of 1.15 eV and 0.75 eV respectively. Configuration with O^{β}-Mo led to the adsorption energy of 0.51 eV. Parallel adsorption (configuration ④) exhibited the lowest adsorption energy of 0.18 eV. Regarding different sites, the adsorption onto the top site led to the highest adsorption energy, followed by SB, LB and hollow sites with adsorption energies of 0.15 eV, 0.16 eV and 0.12 eV respectively. These results predict that FA is more likely to adsorb onto the top site of Mo (110) facet through a single O$^{\alpha}$-Mo (110) bond. EDD was analysed for the adsorption configurations (①, ②, ③) with high adsorption energies to investigate the interface interaction, as shown in Fig. 5.

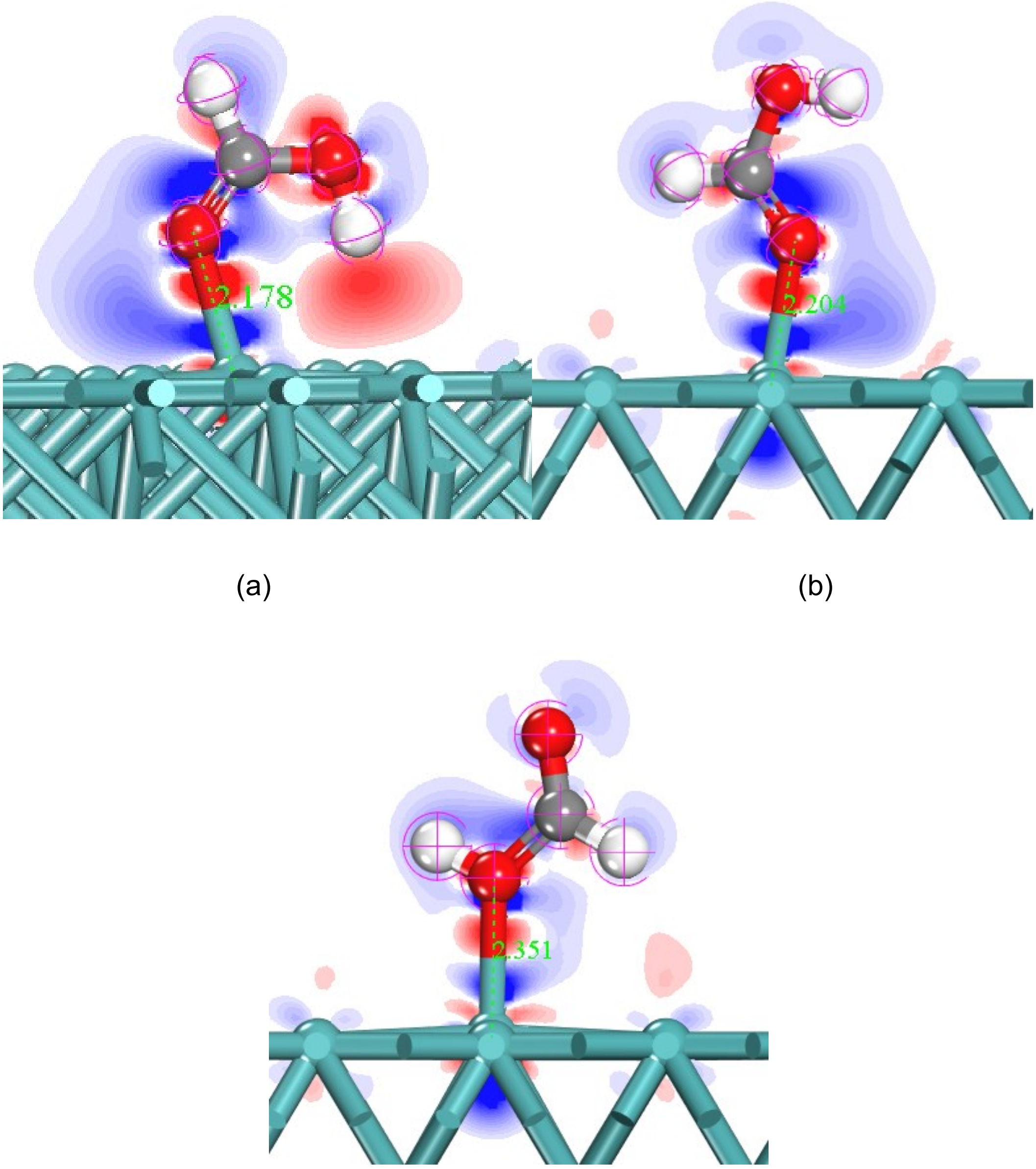

(a) (b)

(c)

Fig. 5. Colour mapping of electron density difference (threshold value: +/- 0.05 electrons/Å^3) for FA adsorption configurations of (a) Top ①, (b) Top ②, and (c) Top ③ (Loss of electrons is indicated in blue, while electron enrichment is indicated in red)

The electron migration exhibited in Fig. 5 indicates that all three adsorption configurations are in the form of chemisorbed species, where O atom locates at the centre of electron migration. Significant electrons migration has been observed for the configuration with O^{α}-Mo bond. Fig. 5(a) shows that strong electron lose has taken place around the O^{α}, but apparently electrons were enriched around O^{α} and O^{β} as well as the hydroxyl hydrogen atom. Similar but minor electron migrations were also observed in the other two cases, as demonstrated in Fig. 5 (b) and (c). The strong electron migration implies large adsorption energy, in line with what has been observed in the AcOH adsorption. However, AcOH leads to mainly electron lose, while the binding between FA molecule and Mo (110) facet is found not only results from electron lose, but also from a strong electron enrichment. This could be ascribed to the electron-donating nature of the methyl in AcOH molecule.

Based on the reaction modelling for the decomposition of FA, the most probable reaction pathways with the lowest energy barriers are shown in Fig. 6, and the bond lengths and bond orders for the FA molecule and its most probable intermediates during the decomposition are presented in Table S4. (a) and (b). The free molecular decomposition of FA in the absence of metal catalyst is also shown in Fig. 3 for comparison.

In the decomposition via the free molecular mechanism, FA showed similar cleavage energy as AcOH for the bond C^{β}-O^{α} (8.59 eV), and slightly lower C-H cleavage energy (4.38 eV) than that of C_{α}-H in AcOH. While the bond C-O^{β} (4.91 eV) and bond O^{β}-H (5.66 eV) were more stable compared to AcOH. All the cleavage reactions in the free molecular decomposition were endothermic as no new bonds were formed.

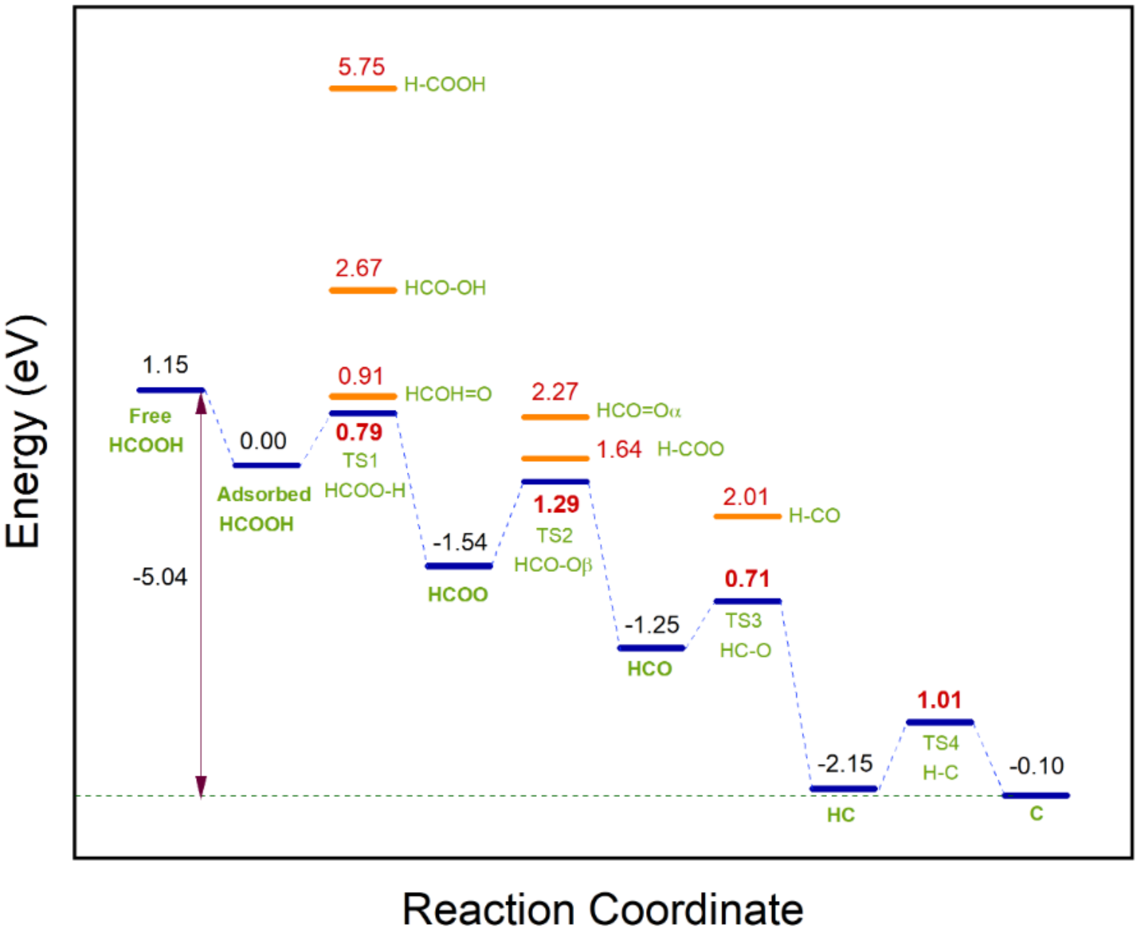

Fig. 6. The decomposition pathways of FA over Mo (110) facet

The decomposition of FA over Mo (110) started by the cleavage of O-H with a small energy barrier of 0.79 eV, and was followed by the cleavage of the bonds C-O$^{\beta}$ and C=O$^{\alpha}$ in sequence with energy barriers of 1.29 eV and 0.71 eV respectively. Finally, the C-H bond cleaved with an energy barrier of 1.01 eV. All the elementary decomposition reactions were exothermic, as shown in Fig. 6.

The modelling results confirm that Mo significantly decreases the cleavage energy of each bond. For instance, the cleavage energy of hydroxyl O-H bond was lowered from 5.66 eV in the free molecular decomposition to 0.79 eV over Mo facet. Besides, the exothermic property of each step in the catalytic decomposition makes it more thermodynamically favoured compared to the free molecular decomposition. The most probable decomposition pathway for FA over Mo facet is HCOOH → HCOO+H →

HCO+O+H → HC+O+O+H → H+C+O+O+H, indicating that O-H and C-H remain the weakest and strongest bond respectively. The highest energy barrier among the elementary reactions was 1.29 eV for the C-O^{β} cleavage, revealing that it is the rate-determining step. When O^{β} is cleaved, the bond between C and the other oxygen (O^{α}) is weakened significantly with the cleavage energy barrier of only 0.71 eV. The cleavage of C=O^{α} was the exothermic reaction with a significant enthalpy change of 2.15 eV. This result indicates that the cleavage of the second C-O bond is the most thermodynamically favoured step for both FA and AcOH. One H atom was released at the beginning of the FA decomposition process and another one at the final step. The single C atom left on the Mo facet might result in carbonaceous deposit or CO_2 generation with additional synthesis reactions [33].

The electron migration within the FA molecule under the effect of Mo is not as significant as that of AcOH. However, the loss of electrons in C=O^{α} still makes it cleave easily prior to C-H bond. The most electron enrichment takes place to the C-O^{β} bond, leading to the highest energy barrier of 1.29 eV for its cleavage reaction.

In the catalytic decomposition of AcOH and FA, Mo causes electron migrations between the interfaces. Consequently most of the bonds in the two acid molecules are significantly weakened. For instance, it was found that both decompositions start with hydroxyl O-H cleavage with much cleavage energy compared to the free molecular decomposition. Besides, the C=O^{α} bonds remain to be the strongest bond in both unabsorbed molecules, but is readily cleaved over Mo facet with much smaller cleavage energy (energy barrier for catalytic reactions), in comparison with the free molecular decomposition. In presence of Mo, AcOH can release two H atoms from hydroxyl and methyl group respectively with low energy barriers, but it requires larger energy to donate another two H atoms from the methylene; the C-H bond becomes stronger when the C was unsaturated inside the molecule. In FA decomposition, the hydroxyl hydrogen is also released at the early stage of its decomposition, however it exhibits higher energy barrier compared to the hydroxyl hydrogen cleavage in AcOH. The other hydrogen in FA is found to be more difficult to release prior to the cleavage of carboxyl oxygen atom, so that it remains to be the final step of the decomposition. The modelling results predict that AcOH possesses a better potential as a hydrogen donor compound over Mo (110) facet.

3.4 Dissociation of H_2 over Mo (110)

The adsorption of H_2 was modelled and the adsorption energy is presented in Table 2. The results reveal that there were only two possible configurations (vertical and parallel) and two probable sites (top and hollow) for H_2 adsorption. The adsorption showed similar adsorption energy in parallel configuration (0.57 eV) and vertical configuration (0.56 eV). A higher adsorption energy of 1.64 eV resulted from the adsorption onto the hollow position, which is the only plausible adsorption position observed in the modelling other than the top position. It is noteworthy that hydrogen molecule was dissociated into two atoms, anchoring on two hollow positions as shown in Fig. 7, known as dissociative adsorption [52]. The overall dissociative adsorption process of H_2 remained to be exothermic.

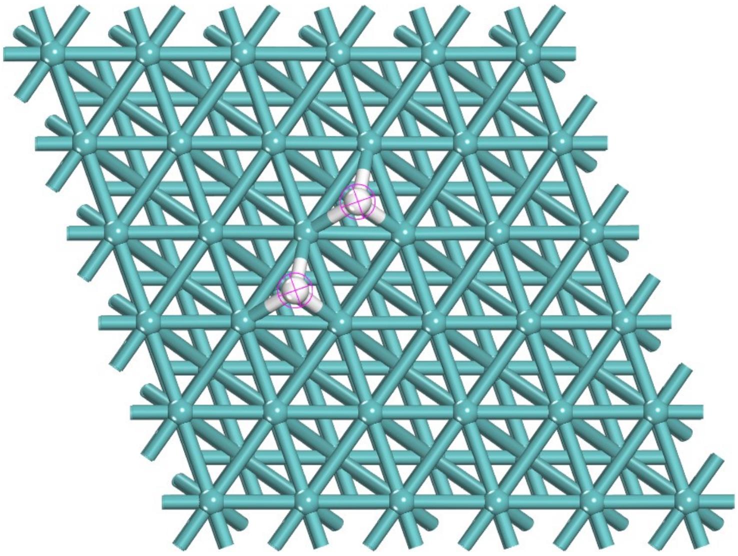

Fig. 7. Configuration of H_2 adsorption onto hollow position

3.5 Comparison of enthalpy changes

Modelling results have predicted that the overall decomposition reactions of AcOH and FA over Mo(110) facet are both exothermic, implying the energy released by new binding formation between their intermediates and the Mo facet is more than the enthalpy change for the old binding cleavage [33,36,39]. Thus, the decomposition of both hydrogen donors over Mo (110) facet is hydrodynamically favoured, similar to the dissociative adsorption of H_2. The enthalpy changes for the adsorption and decomposition of AcOH, FA, and H_2 are calculated respectively, and summarized in Fig. 8.

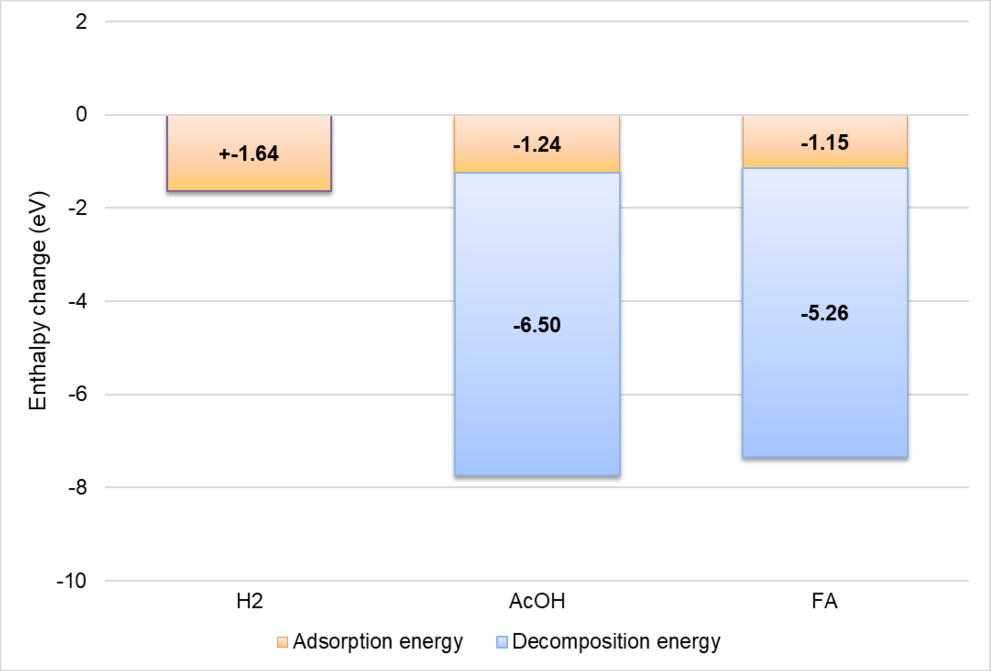

Fig. 8. Overall enthalpy change of adsorption and decomposition of hydrogen donor compounds

Hydrogenation and hydrogenolysis reactions normally happen with single hydrogen migration or spillover during the HDO process [53,54], suggesting that the activation of single hydrogen atom would be an essential step for the hydrogen donation. Therefore, the cleavage of metal-single hydrogen bond plays a key role in such a process. The cleavage (activation) enthalpy of the hydrogen-metal bond is calculated and compared with the adsorption and decomposition enthalpy for each hydrogen donor compound, as shown in Fig. 8.

Additional calculation for the activation of H atom was performed, and the results show that 3.94 eV was required to activate a single hydrogen atom on Mo (110) facet. Previous results predicts that the enthalpy change for the dissociative adsorption of hydrogen molecule is -1.64 eV, which is bigger than those for AcOH and FA (-1.24 eV and -1.15 eV respectively), nevertheless it is inadequate for one single H atom activation. Due to the exothermic decomposition of AcOH and FA, the overall enthalpy change for the bulk adsorption and decomposition process of AcOH and FA were -6.50 eV and -6.19 eV respectively, which are adequate for the activation of H-metal bond. Therefore, the cleavage of H-metal bond could be more facilitated during the decomposition of AcOH and FA. In other words, more hydrogen atoms as well as other decomposed atoms would be likely to migrate and transfer during the decomposition of AcOH and FA compared to the H_2 gas. In this sense, the bio-acids showed good potential to replace H_2 gas as alternative hydrogen donors.

4. Conclusions

The performance of AcOH and FA as hydrogen donors over transition metal facets were investigated and compared with H_2. The adsorption model showed that facets of Ru (0001), Mo (110), Ni (111) and Pd (111) led to the strongest binding to the AcOH molecule among the ten metal facets. Mo (110) was selected as the metal catalyst for further investigating the hydrogen donation of bio-acids as it is a base metal and the lack of atomic-level investigation. EDD analyses revealed that the bindings between bio-acids and Mo were dominated by the electron migration from the molecule to the Mo (110) facet, while electron enrichments in the acid molecule has also been observed for FA adsorption. Mo exhibited positive effect on weakening the bond strength for both acids, and facilitated their cleavage. The reaction model predicted that the most favourable decomposition pathway for acetic acid over Mo (110) was via $CH_3COOH \rightarrow CH_3COO+H \rightarrow CH_3CO+O+H \rightarrow CH_2CO+H+O+H \rightarrow CH_2C+O+H+O+H \rightarrow CHC+H+O+H+O+H \rightarrow CC+2H+O+H+O+H$, where hydroxyl hydrogen and the methyl hydrogen were more readily to be released than the H atoms from the unsaturated methylene. The most favourable decomposition pathway for FA over Mo (110) facet was through $HCOOH \rightarrow HCOO+H \rightarrow HCO+O+H \rightarrow HC+O+O+H \rightarrow H+C+O+O+H$, where the hydroxyl hydrogen can be cleaved and donated at an early stage. Hydrogen showed its undoubtable merits in hydrogen donation because of its dissociative adsorption property over Mo facet. However, compared to the decomposition of H_2 gas, the larger enthalpy change resulted from the exothermic decomposition of the bio-acid compounds would more benefit the activation of decomposed atoms from the catalyst surface, including the hydrogen donation in terms of the single H atom activation and migration. Within the bio-acids, AcOH exhibited a better potential than FA as a hydrogen donor because it released more hydrogen atoms with lower energy barriers. The modelling predicted that AcOH has good potential as an alternative hydrogen donor compound over Mo (110) facet.

Author information

Corresponding Authors

X.Z.: xiaolei.zhang@strath.ac.uk

Author Contributions

All the authors have given approval to the final version of the manuscript.

Notes

The authors declare no competing financial interest.

Acknowledgement

The authors would like to acknowledge financial support from the Leverhulme Trust Research Grant (RPG-2017-254) and EPSRC First Grant (EP/R010986/1). The authors are also grateful for computational support from the UK Materials and Molecular Modelling Hub, which is partially funded by EPSRC (EP/P020194), for which access was obtained via the UKCP consortium and funded by EPSRC grant ref EP/P022561/1.

References

[1] K.M. Isa, T.A.T. Abdullah, U.F.M. Ali, Renew. Sustain. Energy Rev. 81 (2018) 1259–1268.

[2] Z. Si, X. Zhang, C. Wang, L. Ma, R. Dong, Catalysts 7 (2017) 169.

[3] Z. Zhang, C. Wang, X. Gou, H. Chen, K. Chen, X. Lu, P. Ouyang, J. Fu, Appl. Catal. A Gen. 570 (2019) 245–250.

[4] M.J. Gilkey, B. Xu, ACS Catal. 6 (2016) 1420–1436.

[5] K.W. Cheah, M.J. Taylor, A. Osatiashtiani, S.K. Beaumont, D.J. Nowakowski, S. Yusup, A. V. Bridgwater, G. Kyriakou, Catal. Today (2019) 1–11.

[6] Z. Wang, Y. Zeng, W. Lin, W. Song, Int. J. Hydrogen Energy 42 (2017) 21040–21047.

[7] Y. Zeng, Z. Wang, W. Lin, W. Song, Chem. Eng. J. 320 (2017) 55–62.

[8] T. Guo, Q. Xia, Y. Shao, X. Liu, Y. Wang, Appl. Catal. A Gen. 547 (2017) 30–36.

[9] Y. Wang, S. Agarwal, H.J. Heeres, ACS Sustain. Chem. Eng. 5 (2017) 469–480.

[10] E. Vasiliadou, A. Lemonidou, Catalysts 4 (2014) 397–413.

[11] J. Pajak, V. Krebs, J.F. Marêché, G. Furdin, Fuel Process. Technol. 48 (1996) 73–81.

[12] D. Garcìa-Galindo, M. Gòmez-Palmero, M. Lòpez-Palmero, E. Lòpez, F. Sebastian, in: 24th Eur. Biomass Conf. Exhib. 6-9 June 2016, Amsterdam, Netherlands, 2016, pp. 1727–1733.

[13] H. Shafaghat, P.S. Rezaei, W.M.A.W. Daud, J. Taiwan Inst. Chem. Eng. 65 (2016) 91–100.

[14] M. Hosseinpour, S. Fatemi, S.J. Ahmadi, M. Morimoto, M. Akizuki, Y. Oshima, E. Fumoto, Appl. Catal. B Environ. 230 (2018) 91–101.

[15] Q. Song, F. Wang, J. Cai, Y. Wang, J. Zhang, W. Yu, J. Xu, Energy Environ. Sci. 6 (2013) 994.

[16] X. Li, G. Chen, C. Liu, W. Ma, B. Yan, J. Zhang, Renew. Sustain. Energy Rev. 71 (2017) 296–308.

[17] J. Zhang, B. Fidalgo, A. Kolios, D. Shen, S. Gu, Chem. Eng. J. 336 (2018) 211–222.

[18] D. Ballesteros-Plata, A. Infantes-Molina, E. Rodríguez-Castellón, Appl. Catal. A Gen. 580 (2019) 93–101.

[19] M. Pozzo, D. Alfè, Int. J. Hydrogen Energy 34 (2009) 1922–1930.

[20] M. Grilc, B. Likozar, Chem. Eng. J. 330 (2017) 383–397.

[21] S. Ding, Z. Li, F. Li, Z. Wang, J. Li, T. Zhao, H. Lin, C. Chen, Appl. Catal. A Gen. 566 (2018) 146–154.

[22] B. Hočevar, M. Grilc, M. Huš, B. Likozar, Chem. Eng. J. 359 (2019) 1339–1351.

[23] J. Zhang, B. Fidalgo, D. Shen, X. Zhang, S. Gu, Mol. Catal. 454 (2018).

[24] R. Šivec, M. Grilc, M. Huš, B. Likozar, Ind. Eng. Chem. Res. (2019) acs.iecr.9b00898.

[25] W. Luo, A. Asthagiri, J. Phys. Chem. C 118 (2014) 15274–15285.

[26] Z.C. Kramer, X.K. Gu, D.D.Y. Zhou, W.X. Li, R.T. Skodje, J. Phys. Chem. C 118 (2014) 12364–12383.

[27] R. ALCALA, J. Catal. 218 (2003) 178–190.

[28] P. Ferrin, D. Simonetti, S. Kandoi, E. Kunkes, J.A. Dumesic, J.K. Nørskov, M. Mavrikakis, J. Am. Chem. Soc. 131 (2009) 5809–5815.

[29] Y. Choi, P. Liu, Catal. Today 165 (2011) 64–70.

[30] M. Myint, Y. Yan, J.G. Chen, J. Phys. Chem. C 118 (2014) 11340–11349.

[31] F. Gao, Y. Wang, L. Burkholder, C. Hirschmugl, D.K. Saldin, H.C. Poon, D. Sholl, J. James, W.T. Tysoe, Surf. Sci. 602 (2008) 2264–2270.

[32] K. Kim, J. Oh, T.W. Kim, J.H. Park, J.W. Han, Y.-W. Suh, Catal. Sci. Technol. 7 (2017) 3728–3735.

[33] Z. Jiang, P. Qin, T. Fang, Appl. Surf. Sci. 396 (2017) 857–864.

[34] Y. Huang, X. Dong, Y. Yu, M. Zhang, J. Phys. Chem. C 121 (2017) 26733–26741.

[35] M.D. Esrafili, P. Nematollahi, R. Nurazar, Synth. Met. 215 (2016) 164–169.

[36] X. Li, S. Wang, Y. Zhu, G. Yang, P. Zheng, Int. J. Hydrogen Energy 40 (2015) 330–339.

[37] K.I. Gursahani, R. Alcalá, R.D. Cortright, J.A. Dumesic, Appl. Catal. A Gen. 222 (2001) 369–392.

[38] R. Alcala, J.W. Shabaker, G.W. Huber, M.A. Sanchez-Castillo, J.A. Dumesic, J. Phys. Chem. B 109 (2005) 2074–2085.

[39] C. Hu, S.-W. Ting, K.-Y. Chan, W. Huang, Int. J. Hydrogen Energy 37 (2012) 15956–15965.

[40] B. Delley, J. Chem. Phys. 92 (1990) 508–517.

[41] M.D. Segall, P.J.D. Lindan, M.J. Probert, C.J. Pickard, P.J. Hasnip, S.J. Clark, M.C. Payne, J. Phys. Condens. Matter 14 (2002) 2717–2744.

[42] J.P. Perdew, K. Burke, M. Ernzerhof, Phys. Rev. Lett. 77 (1996) 3865–3868.

[43] S. Grimme, J. Comput. Chem. 27 (2006) 1787–1799.

[44] K. Lejaeghere, V. Van Speybroeck, G. Van Oost, S. Cottenier, Crit. Rev. Solid State Mater. Sci. 39 (2014) 1–24.

[45] C.J. Pickard, B. Winkler, R.K. Chen, M.C. Payne, M.H. Lee, J.S. Lin, J.A. White, V. Milman, D. Vanderbilt, Phys. Rev. Lett. 85 (2000) 5122–5125.

[46] I.G. Shuttleworth, Surf. Sci. 661 (2017) 49–59.

[47] F.L. Hirshfeld, Theor. Chim. Acta 44 (1977) 129–138.

[48] M. Grilc, B. Likozar, Chem. Eng. J. 330 (2017) 383–397.

[49] J. Zhang, B. Fidalgo, D. Shen, X. Zhang, S. Gu, Mol. Catal. 454 (2018) 30–37.

[50] A. V. Mironenko, D.G. Vlachos, J. Am. Chem. Soc. 138 (2016) 8104–8113.

[51] B. Pekmezci Karaman, N. Cakiryilmaz, H. Arbag, N. Oktar, G. Dogu, T. Dogu, Int. J. Hydrogen Energy 42 (2017) 26257–26269.

[52] J. Greeley, M. Mavrikakis, J. Phys. Chem. B 109 (2005) 3460–3471.

[53] S. Xia, Z. Yuan, L. Wang, P. Chen, Z. Hou, Appl. Catal. A Gen. 403 (2011) 173–182.

[54] A.M. Doyle, S.K. Shaikhutdinov, S.D. Jackson, H.-J. Freund, Angew. Chemie Int. Ed. 42 (2003) 5240–5243.